

Reducing PEC Overhead by Pauli Error Propagation

Timon Scheiber,^{1,2,*} Paul Haubenwallner,^{1,2} and Matthias Heller^{1,2}

¹*Fraunhofer Institute for Computer Graphics Research IGD*

²*Technical University of Darmstadt, Interactive Graphics Systems Group*

Quantum error mitigation is regarded as a possible path to near-term quantum utility. The methods under the quantum error mitigation umbrella term, such as probabilistic error cancellation, zero-noise extrapolation or Clifford data regression are able to significantly reduce the error for the estimation of expectation values, although at an exponentially scaling cost, i.e., in the sampling overhead. In this work, we present a straightforward method for reducing the sampling overhead of PEC on Clifford circuits (and Clifford subcircuits) via Pauli error propagation alongside some classical preprocessing. While the methods presented in this work are restricted to Clifford circuits, we argue that Clifford sub circuits often occur in relevant calculations as for example the resource state generation in measurement based quantum computing.

I. INTRODUCTION

Quantum computing is expected to outperform classical computing in specific use cases within the near future [1, 2]. However, most of the existing algorithms showing a rigorously proven superior scaling compared to classical algorithms lie beyond the reach of current noisy intermediate scale quantum (NISQ) computers and will probably become relevant only after fault-tolerance is achieved [3, 4]. While recently tremendous progress in the realization of error corrected qubits has been made, both in terms of efficient encodings [5–7], and real hardware demonstrations [7–10], current quantum hardware is still far from being fault-tolerant. On the other side, evidence has been presented that the current generation of quantum hardware can access computational spaces, which might be out of reach even for advanced supercomputers [11–13]. Since these devices are still bound by noise, current NISQ-algorithms require aid by quantum error mitigation (QEM) schemes to be able to compete with classical solutions.

QEM methods mostly focus on quantum algorithms, that aim to estimate the expectation value $\langle A \rangle$ of some observable A , by reducing the noise induced bias at the cost of an increase in the variance of the estimate [14–16]. One of the earlier presented methods is the so-called probabilistic error cancellation (PEC)[17]. PEC aims to construct an ideal, noiseless circuit operation $\mathcal{U}(\rho) = U\rho U^\dagger$ by expanding it into an (over-complete) basis of natively performable, noisy operations \mathcal{O}_i , which can be directly executed by the hardware. This expansion can be achieved in two ways: Either by *compensation*, where each gate operation \mathcal{U}_i of a circuit $\mathcal{U} = \mathcal{U}_n \cdots \mathcal{U}_0$ is directly replaced by the superimposed operation $\mathcal{U}_i = \sum_j \eta_j \mathcal{O}_j$ for some real coefficients η_j , or alternatively by *inversion*, where for each noisy operation $\tilde{\mathcal{U}}_i = \Lambda_i \circ \mathcal{U}_i$ the mathematical inverse of the noise channel $\Lambda_i^{-1} = \sum_j \eta'_j \mathcal{O}_j$ is implemented directly before or after Λ_i to cancel the effect of the noise [18]. The imple-

mentation of this decomposition is performed probabilistically by sampling from a quasi-probability distribution defined by the linear combination with probabilities respecting the weights η_j . This implementation performs the ideal operation on average, but it generally comes at the cost of an increase in the variance of the desired result described by the sampling overhead γ . The latter method has recently been demonstrated experimentally on a superconducting quantum chip [19]. In the reference, a sparse Pauli Lindblad noise model was derived to efficiently characterize and learn device noise and estimate the inverse noise channels Λ_i^{-1} for different layers of noisy two-qubit gates. While the method delivers excellent results in terms of retrieving nearly bias-free estimates, the exponentially scaling increase in γ still limits the usefulness of the method to small circuits.

In this work, we tackle this problem by introducing a method to estimate and sample from a conjoint inverse noise channel (or fused noise channel) $\Lambda_{\text{global}}^{-1}$ in contrast to sampling from each inverse noise channel separately. To estimate this conjoint inverse noise channel we utilize Pauli error propagation through Clifford circuits. We show, that the proposed method can greatly reduce the required sampling overhead.

II. PROBABILISTIC ERROR CANCELLATION FOR PAULI ERRORS

In this section we give a brief overview of PEC by inversion. We assume that the individual noise channels occurring during a quantum operation can be described as an ideal Pauli channel, which can generally be assured by randomized compiling over the Pauli group (also known as Pauli twirling) [20]

$$\Lambda(\rho) = \sum_{i=1}^{N=4^n} c_i P_i \rho P_i^\dagger. \quad (1)$$

The summation runs over all elements P_i of the Pauli group of dimension n , where n denotes the number of qubits. The real, positive channel coefficients c_i sum to

* timon.florian.scheiber@igd.fraunhofer.de

one and can be interpreted as the probability of a Pauli error P_i occurring additionally to the effect of the ideal operation \mathcal{U} . To perform PEC we assume that the exact coefficients of the correlated Pauli errors can be efficiently learned, for example by using techniques such as cycle benchmarking [19, 21].

An important property of Pauli noise channels is that their mathematical inverse also closely resembles a Pauli channel

$$\Lambda^{-1}(\rho) = \sum_{i=1}^N \tilde{c}_i P_i \rho P_i^\dagger, \quad (2)$$

however, with coefficients \tilde{c}_i that are no longer guaranteed to be positive. While not being a channel in the mathematical sense, we will refer to the map defined by eq. 2 as the inverse channel throughout this manuscript. The inverse is in general not a completely positive trace preserving (CPTP) map and can thus not be implemented by a single unitary operation. Its effect can however be realized *probabilistically*.

To implement the operation probabilistically, eq. 2 can be restructured as follows:

$$\Lambda^{-1}(\rho) = \gamma \sum_{i=1}^N \text{sgn}(\tilde{c}_i) \cdot p_i P_i \rho P_i^\dagger, \quad p_i = \frac{|\tilde{c}_i|}{\gamma}, \quad (3)$$

where the factor γ is given by

$$\gamma = \sum_{i=1}^N |\tilde{c}_i|. \quad (4)$$

The benefit of restructuring the inverse channel in this way stems from the fact that the coefficients p_i can now be interpreted as probabilities. Utilizing eq. 3, the inverse is performed *on average* by sampling and applying the Pauli correction P_i directly before the noisy gate with corresponding probability p_i and multiplying the measured expectation value with the corresponding sign $\text{sgn}(\tilde{c}_i) = s_i$ and γ -factor in post-processing.

To apply the method to circuits containing multiple noisy gate operations (or layers of parallel executed operations) $\tilde{\mathcal{U}} = \prod_{l=1}^L (\mathcal{U}_l \circ \Lambda_l)$, this process is repeated for each noisy layer $\tilde{\mathcal{U}}_l$ of the circuit, so that an individual correction is drawn and directly applied in front of the layer. Since each correction is attached to a corresponding sign and sampling overhead, the overall sign $s_{\text{global}} = \prod_l s_l$ and γ -factor $\gamma_{\text{total}} = \prod_l \gamma_l$ for the complete circuit are given by the product of the individual signs and sampling overheads respectively.

To retrieve the expectation value of the mitigated observable, several correction circuit instances are generated and executed. The individual results are multiplied by the total sampling overhead γ_{total} , and the respective global sign s_{global} . Finally, the mitigated expectation value is given by the average of the M executed correc-

tion circuits [17]

$$\langle A \rangle_{\text{ideal}} = \frac{\gamma_{\text{total}}}{M} \sum_{m=1}^M s_{\text{global},m} \langle A \rangle_{\text{corr},m} \quad (5)$$

where $\langle A \rangle_{\text{corr},m} = \text{Tr}(A \tilde{\mathcal{U}}_{\text{corr},m}(\rho))$ refers to the expectation value of A evaluated on the m -th circuit.

As described by van den Berg et al. [19], the factor $\gamma \geq 1$ is directly related to the variance of the mitigated observable, which scales with γ^2 . Since each noisy layer is associated with an individual noise channel, and thus an individual factor γ_l , the total γ -factor of the system increases exponentially. It follows that the variance of the mitigated expectation value and hence the number of shots required for a small sampling error, grows exponentially with the circuit depth.

III. PROPAGATED PROBABILISTIC ERROR CANCELLATION (PPEC) FOR CLIFFORD CIRCUITS

One of the limiting factors of PEC is the large overhead to compensate for the rapid growth in variance. We approach this problem by introducing a straightforward method to decrease the sampling overhead of classical PEC, which we call (error)-propagated probabilistic error cancellation (pPEC). In pPEC the individual inverse noise channels of a given circuit are propagated to the start (or end) of the circuit and multiplied together, yielding a conjoint operation with preferable γ -factor. To estimate this fused inverse noise channel, we present two methods; a hardware-agnostic Monte-Carlo method which serves as a more educational example (see appendix A) as well as an analytic method based on sparse Pauli Lindbladian noise models [19]. We motivate this approach by showing that it is favorable to sample from a conjoint inverse noise channel $\Lambda_{\text{global}}^{-1}$ by comparing the sampling overhead $\gamma_{\text{global}} = \gamma(\Lambda_{\text{global}}^{-1})$ of applying the global inverse (fused noise channel for all layers) to the sampling overhead of correcting each layer individually $\gamma_{\text{total}} = \prod_l \gamma(\Lambda_l^{-1})$.

In a naïve approach to estimate the global noise channel one could try to directly apply a learning procedure to the full circuit which, in the general case, would require an exponentially scaling amount of measurements and is thus infeasible. However, the circuit can be decomposed into a product of individual noisy gate layers $\tilde{\mathcal{U}}_l$, each consisting of a (largely) learnable [22] noise channel Λ_l . It is customary to assume that one qubit operations are effectively noiseless and only the two qubit operation contribute to the noise due to order of magnitude higher errors on most devices. The full circuit operation $\tilde{\mathcal{U}}$ can then be decomposed into a product of noisy circuit operations $\tilde{\mathcal{U}}_l$

$$\tilde{\mathcal{U}} = \prod_l \tilde{\mathcal{U}}_l = \prod_l (\mathcal{U}_l \circ \Lambda_l), \quad (6)$$

where we assume $\Lambda_l = \mathbb{1}$, if \mathcal{U}_l consists solely of single qubit gates. The effect of the noise can be cancelled by probabilistically implementing the inverse of the noise channel Λ_l^{-1} directly before the application of the noisy gate $\tilde{\mathcal{U}}_l$. A graphical depiction of the method is presented in the upper part of Fig. 1.

Since we are only interested in calculating the global inverse noise channel and not the global noise channel itself, we consider the PEC-corrected circuit $\mathcal{U}(\rho) = \prod_{l=1}^L \mathcal{U}_l \Lambda_l \Lambda_l^{-1}$ as a point of departure. From this we can calculate the global inverse by propagating each inverse to the start of the circuit

$$\Lambda_{\text{global}}^{-1} = \prod_{l=L}^1 \tilde{\Lambda}_l^{-1}, \quad (7)$$

where the individual, propagated operations are given by

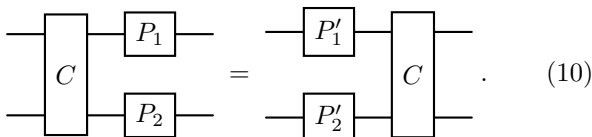
$$\tilde{\Lambda}_l^{-1} = \mathcal{U}_0 \cdots \mathcal{U}_{l-2} \mathcal{U}_{l-1} (\Lambda_l^{-1}), \quad (8)$$

with $\mathcal{U}_j (\Lambda_l^{-1}) = U_j \Lambda_l^{-1} U_j^\dagger$ describing the Heisenberg propagation of the inverse channels. Note that the product runs over the layers in reversed order, and we only conjugate the inverse noise channels with the ideal circuit operations and not the noise channels.

It is important to note, that for arbitrary gates the propagated inverse might not be described by a diagonal (inverse) Pauli channel. A notable exception is however given for the case of the gate conjugation under the Clifford group. This is the case, since elements of the Clifford group are defined by the property that the conjugation of a Pauli gate by a Clifford gate maps the Pauli operator to a different Pauli operator

$$C P C^\dagger = P', \quad (9)$$

where P and P' denote operators of the Pauli group and C an arbitrary operator of the Clifford group. Using eq. 9 we are able to move the Pauli correction terms past a Clifford gate by exchanging it with the conjugated Pauli correction P'



$$\begin{array}{c} \text{---} \\ | \\ \text{---} \end{array} \begin{array}{|c|} \hline C \\ \hline \end{array} \begin{array}{c} \text{---} \\ | \\ \text{---} \end{array} \begin{array}{|c|} \hline P_1 \\ \hline \end{array} \begin{array}{c} \text{---} \\ | \\ \text{---} \end{array} = \begin{array}{c} \text{---} \\ | \\ \text{---} \end{array} \begin{array}{|c|} \hline P'_1 \\ \hline \end{array} \begin{array}{c} \text{---} \\ | \\ \text{---} \end{array} \begin{array}{|c|} \hline C \\ \hline \end{array} \begin{array}{c} \text{---} \\ | \\ \text{---} \end{array} \begin{array}{|c|} \hline P'_2 \\ \hline \end{array} \begin{array}{c} \text{---} \\ | \\ \text{---} \end{array}. \quad (10)$$

In general this conjugation can be performed efficiently by using a look-up table, which we provide in appendix B for the convenience of the reader.

This way the individual channels can be propagated to the start of the circuit and multiplied together yielding the global (inverse) noise channel.

The key advantage of multiplying the individual inverses together before the probabilistic implementation stems from the fact, that different errors or corrections can interfere destructively. The identification of these corrections before applying the inverse probabilistically

can thus reduce the required number of correction circuits by a sometimes large amount. For example, the PEC corrected expectation value with M independently sampled corrections can be expressed as

$$\langle A \rangle_{\text{PEC}} = \frac{\gamma_{\text{total}}}{M} \left[\sum_{m=1}^M s_m \langle A \rangle_{\text{corr},m} \right] \quad (11)$$

where $\langle A \rangle_{\text{corr},m}$ denotes the expectation value of A on the m -th circuit and s_m the corresponding global sign. By now identifying the number of corrections \mathcal{J} that interfere destructively, meaning that the local corrections map to the same global correction with opposite sign, equation 11 can be restructured as

$$\begin{aligned} \langle A \rangle_{\text{PEC}} &= \frac{\gamma_{\text{total}}}{M} \left[\sum_{m=1}^{M-\mathcal{J}} s_m \langle A \rangle_{\text{corr},m} + \underbrace{\sum_{j=1}^{\mathcal{J}} s_j \langle A \rangle_{\text{corr},j}}_0 \right] \\ &= \frac{\gamma_{\text{total}}}{M} \left[\sum_{m=1}^{M-\mathcal{J}} s_m \langle A \rangle_{\text{corr},m} \right] \end{aligned} \quad (12)$$

where, by assumption, the last \mathcal{J} correction circuits interfere destructively meaning that the individual expectation values cancel each other out.

In contrast, by only sampling from the non-interfering corrections, the pPEC corrected expectation value with $M - \mathcal{J}$ independently drawn correction circuits is given by

$$\langle A \rangle_{\text{pPEC}} = \frac{\gamma_{\text{total}}}{M - \mathcal{J}} \left[\sum_{m=1}^{M-\mathcal{J}} s_m \langle A \rangle_{\text{corr},m} \right], \quad (13)$$

which coincides with eq. 12 up to a factor of $\frac{M-\mathcal{J}}{M}$. This factor can then be incorporated into the γ -factor giving the sampling overhead for pPEC

$$\gamma_{\text{pPEC}} = \gamma_{\text{total}} \cdot \frac{M - \mathcal{J}}{M}. \quad (14)$$

Hence, sampling from the pPEC distribution can be seen as sampling from a quasi-probability distribution with reduced sampling overhead γ . The reduction stems from the fact that pPEC is able to identify the interfering corrections before the implementation. We provide a more illustrative example of how the interference of corrections follows from error propagation as well as a method to estimate a fused channel in appendix A. Furthermore, we provide a more rigorous proof that the sampling from the global or fused inverse is always favorable in appendix C.

A. XI-Reduction

To decrease the sampling overhead even further, we reduce the number of individual Pauli corrections that

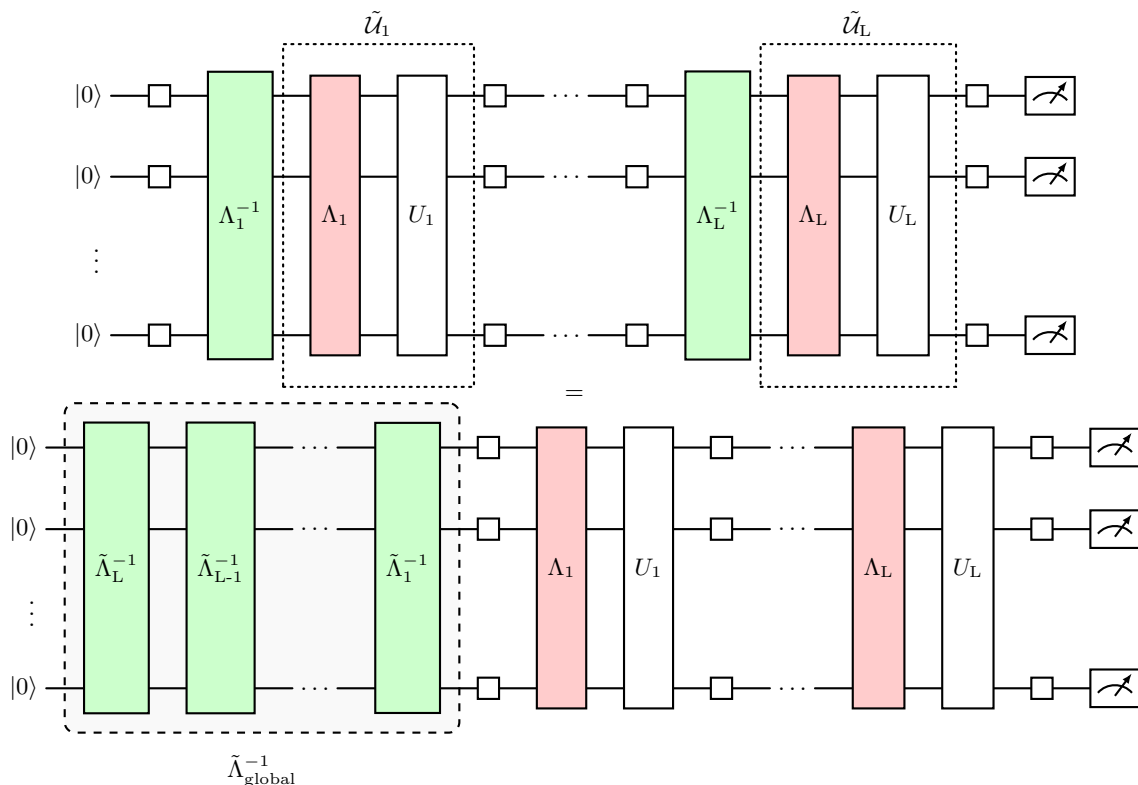


FIG. 1: **Above**, graphical summary of the PEC method. The circuit consists of one qubit gates and layers of noisy two qubit gates $\tilde{U}_i = U_i \circ \Lambda_i$. The noise is probabilistically cancelled by implementing the inverse of the noise channel and applying it in front of the noise. **Below**, the same circuit after propagation of the inverse noise channels to the start of the circuit. After multiplication the full noise of the circuit is cancelled with the single layer correction $\Lambda_{\text{total}}^{-1}$.

need to be applied at the start of the circuit, by utilizing the phase invariance of the computational basis states. Considering for example the Pauli Z operator it is easy to verify that $Z|0\rangle = I|0\rangle$ and $Z|1\rangle = -|1\rangle = I|1\rangle$ (up to a global phase). This allows us to replace each Z operator with an identity operation if applied to a computational basis state without superposition, as for example at the start of the circuit. Furthermore, the Pauli Y operator can be expressed as $Y = -iX \cdot Z$ and thus $Y|0\rangle = X|0\rangle$ and $Y|1\rangle = X|1\rangle$ (omitting the global phase). The conjecture trivially holds for tensorized Paulis, for example the Pauli strings $IXXZY \rightarrow IXXIX$ and $IYYIX \rightarrow IXXIX$ will reduce to the same Pauli string after the reduction and can thus be corrected by the same operation. Using these reductions the total number of corrections and thus the maximum number of instances that need to be sampled individually reduces from 4^n to 2^n .

It is noteworthy that this reduction is inherently symmetric, in the sense that it can be applied either after propagation of the gates to the start or to the end of the circuit, directly before the measurement. This convenience directly follows from Born's rule, stating that only the squared magnitude of the amplitudes can be

measured. For example in the computational basis the measurement of a quantum state $|\psi\rangle = \sum_{i \in \{0,1\}^n} c_i |i\rangle$ will result in the outcome i with probability $|c_i|^2$. Thus, any transformation $c_i \rightarrow e^{i\phi_i} c_i$ does not change the measurement outcome. Note, that the final measurement is always in the computational basis, when incorporating the final basis change into the circuit.

B. Readout-Error-Mitigation

Another common source of errors in quantum circuits are state preparation and measurement (SPAM) errors. Here we utilize PEC for the mitigation of measurement errors and integrate them into the pPEC workflow. The readout error mitigation method presented in this work is based on so-called assignment matrix inversion methods [23–25]. In these methods an assignment matrix A is calculated by preparing each basis state individually and measuring the noisy outcome. The matrix A correlates the ideal measurements with the noisy measurements via the relation $\vec{p}_{\text{noisy}} = A\vec{p}_{\text{ideal}}$. The idealized counts can then be retrieved by inverting the assignment matrix and multiplying the experimentally retrieved probability vector of the bit-strings with the inverted assignment matrix

$\vec{p}_{\text{ideal}} = A^{-1}\vec{p}_{\text{noisy}}$. While this method almost fully eliminates readout errors, an exponential overhead for the preparation of the 2^n basis states is introduced, rendering the method infeasible for larger circuits.

To reduce this overhead we depart from this model and assume a tensor product noise model as presented in ref. [23]

$$A = \bigotimes_{i=1}^n A^i = \bigotimes_{i=1}^n \begin{bmatrix} 1 - \epsilon_i & \eta_i \\ \epsilon_i & 1 - \eta_i \end{bmatrix}, \quad (15)$$

with ϵ_i and η_i denoting the $|0\rangle \rightarrow 1$ and $|1\rangle \rightarrow 0$ faulty readout probabilities on qubit i respectively. This imposes a significant simplification, but it can be considered reasonable for sparse measurement outcomes [26]. The tensor product of eq. 15 runs over the individual 2×2 assignment matrices, which are defined for each individual qubit. These matrices are generally not equal among the qubits nor symmetrical under transposition, meaning that the individual bit-flip probabilities for $|0\rangle \rightarrow 1$ and $|1\rangle \rightarrow 0$ are not identical.

To apply the PEC method in a fashion that integrates to the pPEC framework, we wish to construct a measurement error channel that closely resembles a Pauli channel. This is achieved by symmetrizing the matrices A^i via randomized insertion of X gates [27]. Hereby an X gate is drawn and applied with 50% probability directly before the measurement and corrected in post-processing. This procedure symmetrizes the matrix $A_{\text{twirl}}^i = (A_{\text{twirl}}^i)^T$ (see appendix D) which can then be described by an X channel. This allows us to write the individual measurement error channel in the form

$$\Pi_{\text{meas}}(\rho) = \sum_m (1 - p_x) \pi_m I \rho I \pi_m + p_x \pi_m X \rho X \pi_m, \quad (16)$$

where the π_m are projection operators, fulfilling the relations $\pi_m \pi_{m'} = \delta_{mm'} \pi_m$, $\pi_m = \pi_m^\dagger$ and $\sum_m \pi_m = I$. The bit-flip probabilities are explicitly given by the arithmetic average of the individual bit-flip probabilities, $p_{x,i} = \frac{\epsilon_i + \eta_i}{2}$.

IV. NUMERICAL SIMULATIONS

Due to the large shot budget (and time reservation) required to fully characterize the complete noise channels we restrict the experiments to numerical simulations. Since pPEC does not rely on approximations it is expected that the performance will be similar to regular PEC.

A. Gate level noise

To demonstrate the efficiency of our proposed method, we compare PEC and pPEC for a random 10 qubit circuit consisting of Hadamard (H), Pauli (X, Y, Z), phase

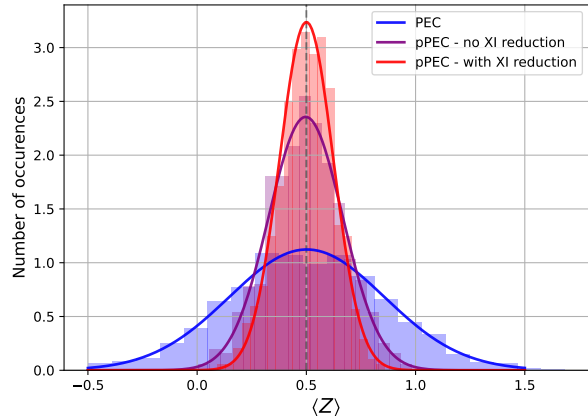


FIG. 2: Mitigated circuits for the three tested method, PEC (blue), pPEC (purple), pPEC with XI-reduction (red). All methods are able to retrieve error free estimates of the noiseless observable. pPEC generally leads to smaller variances than the direct approach.

(S), controlled phase (C_Z) and measurement operations under gate level noise. For each two-qubit gate we apply a depolarizing channel

$$\Lambda_{\text{depol}}(\rho) = (1 - p)I\rho I + \frac{p}{(N - 1)} \sum_{i=2}^{N=4^2} P_i \rho P_i^\dagger, \quad (17)$$

where we chose the error probability $p \approx 2\%$ to resemble current hardware error rates [19]. It should be noted that processes such as hardware specific idle times of qubits which generally lead to dephasing and decay are not modeled in this description. Additionally, we integrate a tensor product, asymmetric readout error with a mean of $p_{\text{read}} \approx 2\%$, which we symmetrize via the method we introduced in sec. III B.

Using a random Clifford circuit we benchmark the three different PEC protocols – PEC, pPEC and pPEC with XI-reduction. We perform the method by drawing corrections from each inverse noise channel directly (PEC) or by drawing from the pPEC distribution. For the considered example the pPEC circuits have been calculated by the direct product of all channels, which is generally possible for circuits with modest numbers of qubits. For larger circuits the same can be done, however the product needs to be truncated as the space of possible corrections grows exponentially. From each of these distributions a total of 40 correction circuits is drawn, which are simulated with 1024 shots per circuit instance.

To obtain a sufficient amount of statistics a sample with a total of 1000 mitigated expectation values per method was generated. The resulting distribution is presented in fig. 2. As expected, all PEC methods are able to retrieve the bias free expectation value on average, although at vastly different variances. Due to the promis-

ing results we now explore the scaling of the different approaches.

To investigate the expected scaling, we benchmark the methods by calculating the global inverse for a sample of random 5-qubit Clifford circuits for an increasing number of noisy two-qubit operations and calculate the expected γ -factors. The estimated total γ -factors for the direct PEC, propagated PEC and propagated PEC with XI-reduction are presented in figure 3. Since the sampling-overhead scales exponentially in the number of noisy operations, the data is plotted logarithmically. We achieve a far more favorable scaling for the propagated approach and a further decrease with the XI-reduction. However, it should be noted that the expected reduction can generally depend on the noise and structure of the circuit.

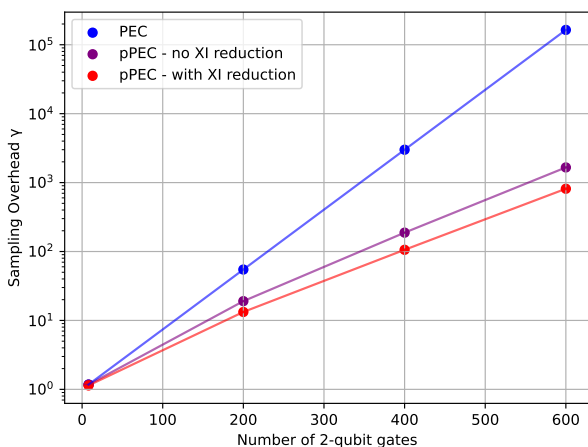


FIG. 3: Calculated Sampling overhead averaged over 100 instances of random 5-qubit Clifford circuits at an increasing number of noisy operations.

B. Circuit level noise with SPL noise model

Sparse Pauli Lindbladian (SPL) models are a recently introduced form of noise model to efficiently capture the noise of devices with limited physical qubit connectivity [19]. In the SPL model the noise is generated by a dissipative Lindbladian of the form $\mathcal{L}(\rho) = \sum_{k \in \mathcal{K}} \lambda_k (P_k \rho P_k^\dagger - \rho)$ with model coefficients λ_k and Lindblad jump operators P_k given by a sparse subset \mathcal{K} of the Pauli group. A noise channel, for a full layer of in-parallel executable gates is then described by the formula

$$\Lambda(\rho) = \prod_{k \in \mathcal{K}} (w_k \mathcal{I}(\cdot) + (1 - w_k) \mathcal{P}_k(\cdot)) \rho, \quad (18)$$

where the coefficients w_k are given by $w_k = (1 + e^{-2\lambda_k})/2$. The product runs over the indexed set \mathcal{K} with far fewer terms than the dense noise model $|\mathcal{K}| \ll 4^n$. \mathcal{K} can be

chosen in a way that only Pauli strings with none identity terms on at most two (physically connected) qubits are present. $\mathcal{P}_i(\cdot) \triangleq P_i \cdot P_i^\dagger$ is a shorthand notation for a single Pauli channel in Kraus representation and the \cdot symbol is a placeholder to illustrate that the whole product is applied to the system's density operator ρ .

We simulate a device with a linear qubit topology, meaning that we choose the model Paulis in eq. 18 by choosing weight two (one) Pauli strings with non-identity terms only on nearest neighbor qubits.

As noise model we consider a quasi depolarizing channel by choosing the coefficients w_k to be homogenous, allowing for easy tuning of the noise strength. We adjust the strength in accordance to the highest reported Pauli fidelity reported in ref. [19], $f_{\max} \approx 0.996$, by utilizing $w_k = \frac{1+f_k}{2}$ where $f_k = \frac{1}{2^n} \text{Tr}(P_k^\dagger \Lambda(P_k))$ is the Pauli fidelity for Pauli P_k with respect to the noise channel Λ .

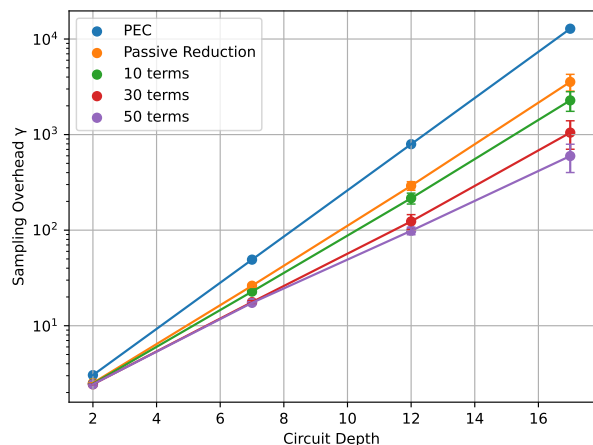


FIG. 4: Calculated γ factors for quantum circuits of increasing circuit depth consisting of 10 qubits with an average Pauli fidelity of $f_{\text{avg}} = 0.996$. The results are averaged over 100 instances of random circuit instances, error bars indicate one standard deviation. The more channels are expanded, the higher the reduction in the sampling overhead γ is achieved, however at an increase in the classical preprocessing cost.

We present the results of pPEC with XI reduction for random Clifford circuits of increasing depth in figure 4. In contrast to the direct multiplications the individual channels, we first construct the global inverse channel in product form, which we expand term by term to reduce the sampling overhead. We find that for the SPL model the XI reduction leads to the vanishing of terms which contain only Z and I operations, which we denote as passive reduction. The details on how pPEC is applied to the SPL noise model are presented in appendix E.

It is important to note that the ordering in which this

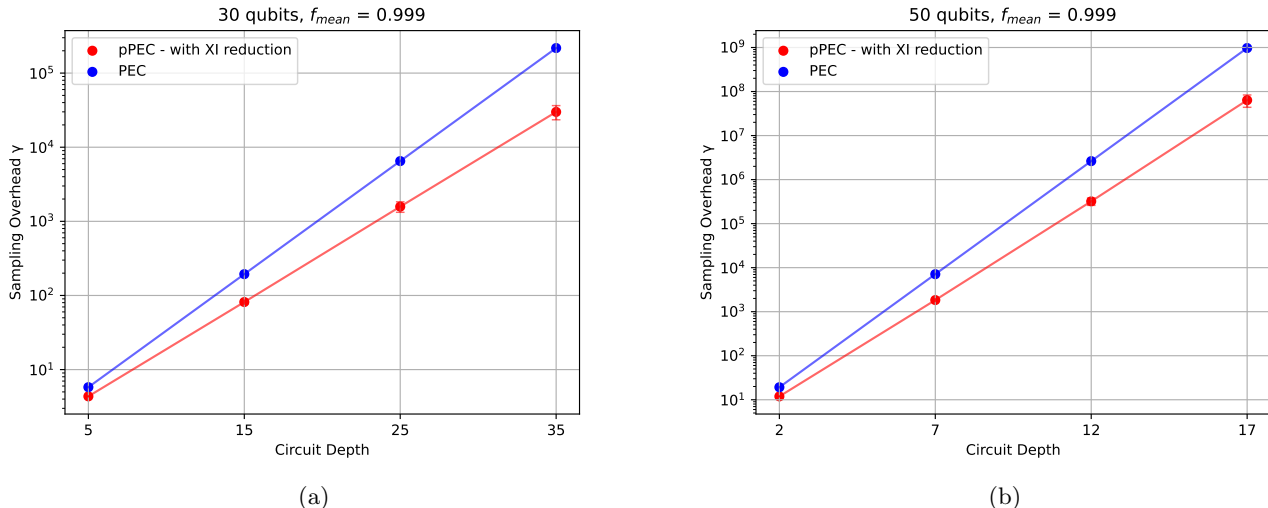


FIG. 5: Performance of pPEC with XI reduction for future devices at (a) 30 qubits and (b) 50 qubits. The results are averaged over 100 random circuit instances with error bars indicating one standard deviation. The amount of expanded channels was taken dynamically, ranging from 0 (lowest depth) to 200 (highest depth).

expansion is performed is crucial to obtain meaningful reductions. Due to the large sampling overhead for the considered device noise we limit the investigation to 10 qubits. The data for higher qubit counts and lower error rates – as expected for future generations of hardware – is presented in figure 5.

Fig 4 shows a clearly favorable scaling relative to direct PEC, reaching an improvement of an order of magnitude even for modest depths. On the other hand a direct comparison to figure 5 shows that the effect of pPEC is far less drastic for lower error rates. We attribute this to the fact, that the amount of interference is generally proportional to the magnitude of the channel coefficients $(1 - w_k)$. For lower error rates the magnitude will not be as large and thus deeper circuits are required to achieve comparable results. However, even for larger circuits and modest depths a noticeable reduction in the sampling overhead can be achieved. We therefore conjecture that pPEC is a practical approach to reduce the amount of quantum resources, as it is always favorable in comparison to direct PEC.

We now consider possible relevant applications in which pPEC might be applicable and help reduce the workload of the quantum computer.

V. POSSIBLE APPLICATIONS

As described in the prior sections, the presented method is only applicable to quantum circuits consisting of Clifford gates. While Clifford circuits themselves are not of any practical relevance due to their efficient simulability via the stabilizer formalism [28], larger Clif-

ford structures do occur in many quantum circuits. In this section we give a brief overview of some possible applications of the proposed method. Since the reduction is generally dependent on the structure of the noise and device, we do not provide a detailed scaling analysis here and give only exemplary results of the reductions that are to be expected.

A. Clifford structures in Quantum Circuits

1. Trotterized quantum simulation

An often occurring Clifford subcircuit is given in the implementation of Pauli exponentials. As an example we consider dynamic quantum simulation where the physical time evolution of a system $|\psi(t = t_0)\rangle$ interacting according to a Hamiltonian H is performed using the unitary time evolution operator

$$U(t_0, t_1) = e^{-iH(t_1 - t_0)} \quad (19)$$

with which the state at time t_1 can be calculated by

$$|\psi(t_1)\rangle = U(t_0, t_1) |\psi(t_0)\rangle. \quad (20)$$

To implement this evolution on a quantum computer the Hamiltonian is usually decomposed into a weighted Pauli sum $H = \sum_j c_j P_j$, which is always possible since the Pauli operators form a basis of the Hilbert space. Since the direct implementation of the sum representation is still not straight forward the operator needs to be further decomposed.

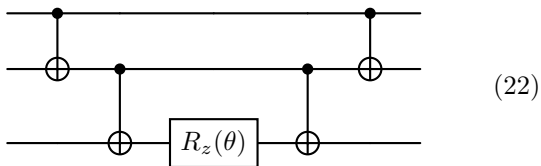
By utilizing the first order Trotter-Suzuki formula [29, 30] the time evolution operator can be decomposed into

several discrete time steps $U(t_0, t_1) \approx \prod_{d=1}^D U_1(\Delta t)$ with the operator $U_1(\Delta t)$ denoting the first order Trotter operator given by

$$U_1(\Delta t) = \prod_{j=1}^N e^{-ic_j P_j \Delta t} \quad (21)$$

and $D = (t_1 - t_0)/\Delta t$ the number of discrete time steps. The implementation of the time evolution can thus be reduced to the physical implementation of the exponentiation of the set of Pauli operators P_j .

These operators can be implemented using a specific Clifford structure, a so-called C_X -ladder. For example, the exponentiation of the Pauli ZZZ operator $\exp(-i\theta/2 \cdot ZZZ)$ can be implemented by the circuit



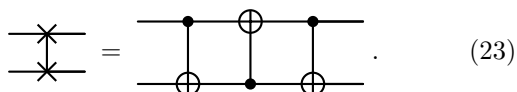
which consists of a single non Clifford gate $R_z(\theta)$ among two C_X ladders. For higher weight Pauli strings the amount of C_X gates grows linearly, providing a Clifford subcircuit on which the pPEC algorithm can be performed, since these operations can be applied at any given circuit section, the XI-reduction can not be applied in general.

Considering a C_X ladder consisting of 10 qubits on a linearly connected device we find, for an average Pauli fidelity of $f_{\text{avg}} = 0.996$, a γ -factor of $\gamma_{\text{PEC}} \approx 58.2$. With pPEC this can be reduced to $\gamma_{\text{pPEC}} \approx 47.14$ which is a reduction by roughly 20%. For large numbers of Pauli exponentials this can lead to considerable reductions.

We further consider the case for improved device fidelities with average $f_{\text{avg}} = 0.9996$ and a C_X ladder of about 30 qubits. In this case we achieve for $\gamma_{\text{PEC}} \approx 62.1$ a reduction of only about 10%, which can still lead to reasonable reductions for several C_X ladders.

2. Increased device connectivity

For devices with sparse qubit connectivities, as for example superconducting quantum computers, interactions of physical qubits that are spatially separated need to be bridged by SWAP gates. SWAP gates are an inherent element of the Clifford group as they can be decomposed to three consecutive C_X -gates



Since these gates cannot be applied in parallel each C_X -gate would contribute with an individual noise channel

Λ_i , which can be reduced with pPEC.

Furthermore, SWAP gates are favorable for pPEC because the conjugation of a model Pauli does not change the weight of the Pauli string, i.e. the amount of non identity terms in a Pauli string stays invariant (see app. B). For layers of swap gates comparable results to the C_X -ladder can be expected.

3. Reducing state preparations in VQE

Another interesting possible application in near-term quantum algorithms is given in minimizing the number of state preparations in the Variational Quantum Eigensolver (VQE) [31]. The VQE algorithm aims to estimate the minimum eigenvalue of a given hermitian matrix H by preparing a parametrized state $|\psi(\theta_1, \theta_2, \dots, \theta_n)\rangle = |\psi(\boldsymbol{\theta})\rangle$ and iteratively minimizing the measured energy

$$E = \min_{\boldsymbol{\theta}} \langle \psi(\boldsymbol{\theta}) | H | \psi(\boldsymbol{\theta}) \rangle \quad (24)$$

by optimizing the parameters of the trial wave function. The optimization is performed via a classical optimization loop, whereas the quantum computer is used to estimate the energy of each generation of parameters. A limitation of this method is the required number of state preparations needed to measure a single instance of $\langle \psi(\boldsymbol{\theta}) | H | \psi(\boldsymbol{\theta}) \rangle$. Usually the matrix H is expressed as a weighted Pauli sum $\sum_j c_j P_j$ so that the total energy estimate reduces to estimating each individual Pauli expectation value separately. For large numbers of Pauli terms the number of required measurements (and therefore state preparations) can rapidly become prohibitive.

The method presented ref. [32] aims to reduce the number of state preparations by grouping the Pauli operators into commuting groups which can be measured in parallel.

To measure the operators within a single state preparation the circuit is mapped to a simultaneous eigenbasis of the group of commuting operators. The basis change, consist entirely of Clifford gates (as expected for a mapping from Pauli operators to Pauli operators), is applied right before the measurement rendering these circuits ideal for pPEC.

As an example the mapping of the mutually commuting Pauli strings $XXXX$, $XYYY$, $YXYX$, $YXXY$ to the basis $ZIII$, $IZII$, $IIZI$, $IIIZ$ is depicted in fig. 6. With the priorly described noise model with an average Pauli fidelity of $f_{\text{avg}} = 0.996$ on a linear device topology we find an approximate $\gamma = 12.696$ for regular PEC.

Alternatively our method results in a γ -factor of 7.335 for pPEC without the XI-reduction as well as $\gamma_{\text{pPEC}_{XI}} = 5.449$ with XI reduction, which is about an order of magnitude improvement in the variance γ^2 .

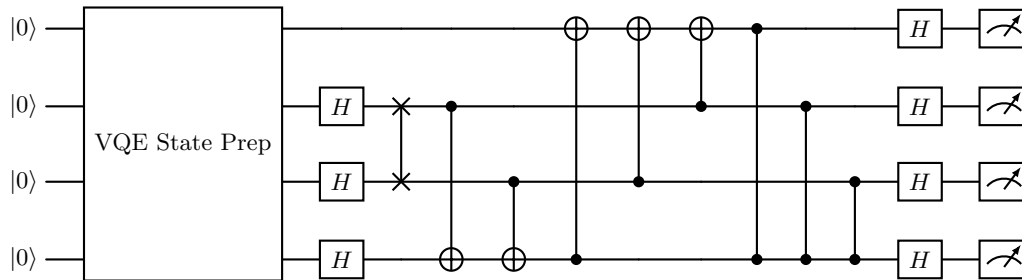


FIG. 6: Example circuit consisting of a state preparation and change into the simultaneous eigenbasis of the Pauli operators $XXXX$, $XXYY$, $XYXY$ and $YXXY$ as presented in ref. [32]. The state preparation prepares a possible ground state wave function according to some ansatz. The measurement basis is then rotated by a Clifford circuit to a basis where the observables of interest can be measured in parallel.

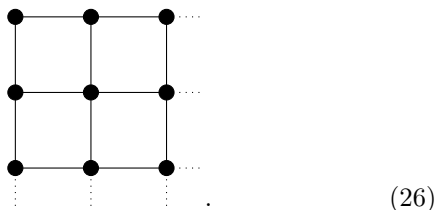
B. Measurement-based quantum computing

The application of pPEC in the model of measurement-based quantum computing (MBQC) [33] presents itself as another interesting possibility. In MBQC the computation is performed on a large, entangled resource state (in this example a graph state), realized by only Clifford operations

$$|G\rangle = \prod_{i,j \in E} C_{Zij} |+\rangle^{\otimes n}. \quad (25)$$

The state is constructed according to a graph $G = (V, E)$, where the vertices correspond to the individual qubits and the edges define which qubits are entangled via C_Z gates. To perform the computation the individual qubits are measured in adaptive bases, performed by the transformation $M(\theta) = HR_z(\theta)$ which is equivalent to the implementation of a gate operation on the resource state. The randomness of a quantum measurement is compensated for by using classically controlled feed-forward operations.

We consider a two-dimensional lattice as a resource state, which is universal for MBQC [34]. This graph is interesting since it can be implemented in constant depth, with a minimum depth of 4 if the device is sufficiently connected



We again consider a device with a limited, linear connectivity and an average Pauli fidelity of $f_{\text{avg}} = 0.996$. For the circuit to implement a graph state described by a 4×4 lattice (transpiled onto the hardware connectivity) we find a γ -factor of regular PEC of approximately

$\gamma_{\text{PEC}} \approx 4899.6$. Using pPEC we are able to reduce this factor to approximately $\gamma_{\text{pPEC}_{X_I}} \approx 839.1$. For improved fidelities $f_{\text{avg}} = 0.9996$ and a 7×7 graph we find $\gamma_{\text{PEC}} \approx 418.8$ and $\gamma_{\text{pPEC}_{X_I}} \approx 324.9$ which is a still considerable improvement of about 20%.

MBQC presents itself as an especially interesting application since the resource state contains all noisy two-qubit operations while only consisting of Clifford gates. Thus, pPEC including the XI-reduction can be applied to the resource state preparation yielding favorable scaling in comparison to PEC. Further, pPEC can be applied to correct for the readout errors that occur during the measurement process. Note that due to the feed-forward operation, assignment matrix methods can generally not be utilized, rendering a PEC approach practical [35].

Considering the structure of the circuits, and the fact that measurement errors are, under symmetrization, defined by an X -channel, it is possible to propagate these errors to the start of the circuit. This is possible since the Pauli X can be pushed behind the H gate changing it to a Z -channel. Since the Pauli Z commutes with $R_z(\theta)$ the measurement errors can be freely propagated through the circuit, allowing us to incorporate them as well into the pPEC workflow.

C. Further possible applications

Apart from the discussed circuits the method can be applied whenever Clifford circuits appear in circuits of practical interest. Possible algorithms could be given by Clifford preconditioning of circuits [36] or applications in IQP circuits [37]. We do not explicitly investigate these approaches here but like to hold them as interesting points of further research.

VI. DISCUSSION AND CONCLUSION

Quantum error mitigation is a promising avenue of investigation to achieve a near future quantum advantage. Even though tremendous progress in hardware error rates has been achieved, QEM is still vital to obtain meaningful results on current hardware. However, one of the limiting factors for error mitigation lies still in the excessive amount of quantum resources required to mitigate large circuits.

In this work we presented a method to, in some cases drastically, reduce the sampling overhead of PEC for Clifford circuits. PEC in combination with Pauli error propagation is able to retrieve bias free expectation values of noisy circuits. The method itself delivers excellent results for current hardware error rates, reducing the sampling overhead by a few orders of magnitude for even moderately deep quantum circuits. We observed that the effect is far less drastic for reduced error rates as is expected for future quantum device generations. However, even for future hardware error rates and quantum circuits consisting of 30-50 qubits a reduction of 1 to 2 orders of magnitude can be achieved, making pPEC an attractive choice whenever possible.

Apart from pPEC recent publications also utilize error cancellation via a global channel implicitly in the context of tensor networks [38]. We hope that the promising results of sampling from a fused inverse could spark further insights in the most effective form of cancelling quantum noise. How to optimally estimate and sample from the global inverse is an interesting question for future research.

The clear bottleneck of our algorithm is the classical overhead to calculate the channel products. We showed that the expansion can be performed without tremen-

dous overhead by truncation, yielding more limited results. A further interesting approach to efficiently expand the noise channel could be given by tensor network algorithms, which can approximate a large amount of data with few resources. By expressing the channels as matrix product operators (MPO) the channel products can be calculated as a contraction of several MPOs [39, 40]. The main problem lies in the fact that, to keep the bond dimension small, approximations need to be made which can lead to a bias in the estimated expectation values. Nonetheless, we consider MPOs as a promising path of further investigation.

Finally, we provided basic examples of possible applications for our presented method, where Clifford circuits – even though they are efficiently simulatable via the Gottesman-Knill-Theorem – are of practical interest. We consider the investigation of MBQC an interesting possibility of further research, especially under consideration of qubit recycling.

We have recently become aware that a recent related publication also employs error propagation to reduce the sampling overhead of PEC [41]. In contrast to our work, the reference considers so called cat-qubits with dominant phase errors and a gate set of bias preserving gates.

ACKNOWLEDGMENTS

This work was in part supported by the research project Zentrum für Angewandtes Quantencomputing (ZAQC), which is funded by the Hessian Ministry for Digital Strategy and Innovation and the Hessian Ministry of Higher Education, Research and the Arts and the research project Leistungszentrum für innovative Therapeutika (TheraNova), which is funded by the Fraunhofer Gesellschaft and the Hessian Ministry for Higher Education, Research and the Arts.

-
- [1] A. J. Daley, I. Bloch, C. Kokail, S. Flannigan, N. Pearson, M. Troyer, and P. Zoller, *Nature* **607**, 667 (2022).
 - [2] A. Di Meglio, K. Jansen, I. Tavernelli, C. Alexandrou, S. Arunachalam, C. W. Bauer, K. Borrás, S. Carrazza, A. Crippa, V. Croft, *et al.*, arXiv preprint arXiv:2307.03236 (2023).
 - [3] C. Gidney and M. Ekerå, *Quantum* **5**, 433 (2021).
 - [4] M. Reiher, N. Wiebe, K. M. Svore, D. Wecker, and M. Troyer, *Proceedings of the national academy of sciences* **114**, 7555 (2017).
 - [5] S. Bravyi, A. W. Cross, J. M. Gambetta, D. Maslov, P. Rall, and T. J. Yoder, *Nature* **627**, 778 (2024).
 - [6] Q. Xu, J. P. Bonilla Ataides, C. A. Pattison, N. Raveendran, D. Bluvstein, J. Wurtz, B. Vasić, M. D. Lukin, L. Jiang, and H. Zhou, *Nature Physics*, 1 (2024).
 - [7] D. Bluvstein, S. J. Evered, A. A. Geim, S. H. Li, H. Zhou, T. Manovitz, S. Ebadi, M. Cain, M. Kalinowski, D. Hangleiter, *et al.*, *Nature* **626**, 58 (2024).
 - [8] V. Sivak, A. Eickbusch, B. Royer, S. Singh, I. Tsioutsios, S. Ganjam, A. Miano, B. Brock, A. Ding, L. Frunzio, *et al.*, *Nature* **616**, 50 (2023).
 - [9] G. Q. AI, *Nature* **614**, 676 (2023).
 - [10] R. Acharya, L. Aghababaie-Beni, I. Aleiner, T. I. Andersen, M. Ansmann, F. Arute, K. Arya, A. Asfaw, N. Astrakhantsev, J. Atalaya, *et al.*, arXiv preprint arXiv:2408.13687 (2024).
 - [11] A. Morvan, B. Villalonga, X. Mi, S. Mandra, A. Bengtsson, P. Klimov, Z. Chen, S. Hong, C. Erickson, I. Drozdov, *et al.*, arXiv preprint arXiv:2304.11119 (2023).
 - [12] Y. Kim, A. Eddins, S. Anand, K. X. Wei, E. Van Den Berg, S. Rosenblatt, H. Nayfeh, Y. Wu, M. Zaletel, K. Temme, *et al.*, *Nature* **618**, 500 (2023).
 - [13] K. Shinjo, K. Seki, T. Shirakawa, R.-Y. Sun, and S. Yunoki, arXiv preprint arXiv:2403.16718 (2024).
 - [14] Z. Cai, R. Babbush, S. C. Benjamin, S. Endo, W. J. Huggins, Y. Li, J. R. McClean, and T. E. O’Brien, *Reviews of Modern Physics* **95**, 045005 (2023).
 - [15] Y. Quek, D. Stilck França, S. Khatri, J. J. Meyer, and

- J. Eisert, *Nature Physics* **20**, 1648 (2024).
- [16] R. Takagi, S. Endo, S. Minagawa, and M. Gu, *npj Quantum Information* **8**, 114 (2022).
- [17] K. Temme, S. Bravyi, and J. M. Gambetta, *Physical review letters* **119**, 180509 (2017).
- [18] S. Endo, S. C. Benjamin, and Y. Li, *Physical Review X* **8**, 031027 (2018).
- [19] E. Van Den Berg, Z. K. Mineev, A. Kandala, and K. Temme, *Nature Physics*, 1 (2023).
- [20] J. J. Wallman and J. Emerson, *Physical Review A* **94**, 052325 (2016).
- [21] A. Erhard, J. J. Wallman, L. Postler, M. Meth, R. Stricker, E. A. Martinez, P. Schindler, T. Monz, J. Emerson, and R. Blatt, *Nature communications* **10**, 5347 (2019).
- [22] S. Chen, Y. Liu, M. Otten, A. Seif, B. Fefferman, and L. Jiang, *Nature Communications* **14**, 52 (2023).
- [23] S. Bravyi, S. Sheldon, A. Kandala, D. C. McKay, and J. M. Gambetta, *Physical Review A* **103**, 042605 (2021).
- [24] P. D. Nation, H. Kang, N. Sundaresan, and J. M. Gambetta, *PRX Quantum* **2**, 040326 (2021).
- [25] L. Funcke, T. Hartung, K. Jansen, S. Kühn, P. Stornati, and X. Wang, *Physical Review A* **105**, 062404 (2022).
- [26] B. Yang, R. Raymond, and S. Uno, *Physical Review A* **106**, 012423 (2022).
- [27] E. Van Den Berg, Z. K. Mineev, and K. Temme, *Physical Review A* **105**, 032620 (2022).
- [28] D. Gottesman, arXiv preprint quant-ph/9807006 (1998).
- [29] H. F. Trotter, *Proceedings of the American Mathematical Society* **10**, 545 (1959).
- [30] M. Suzuki, *Communications in Mathematical Physics* **51**, 183 (1976).
- [31] A. Peruzzo, J. McClean, P. Shadbolt, M.-H. Yung, X.-Q. Zhou, P. J. Love, A. Aspuru-Guzik, and J. L. O'Brien, *Nature communications* **5**, 4213 (2014).
- [32] P. Gokhale, O. Angiuli, Y. Ding, K. Gui, T. Tomesh, M. Suchara, M. Martonosi, and F. T. Chong, arXiv preprint arXiv:1907.13623 (2019).
- [33] H. J. Briegel, D. E. Browne, W. Dür, R. Raussendorf, and M. Van den Nest, *Nature Physics* **5**, 19 (2009).
- [34] R. Raussendorf, D. E. Browne, and H. J. Briegel, *Physical review A* **68**, 022312 (2003).
- [35] R. S. Gupta, E. Van Den Berg, M. Takita, D. Riste, K. Temme, and A. Kandala, *Physical Review A* **109**, 062617 (2024).
- [36] J. Sun, L. Cheng, and W. Li, *Journal of Chemical Theory and Computation* **20**, 695 (2024).
- [37] D. Shepherd and M. J. Bremner, *Proceedings of the Royal Society A: Mathematical, Physical and Engineering Sciences* **465**, 1413 (2009).
- [38] S. Filippov, M. Leahy, M. A. Rossi, and G. García-Pérez, arXiv preprint arXiv:2307.11740 (2023).
- [39] C. J. Wood, J. D. Biamonte, and D. G. Cory, arXiv preprint arXiv:1111.6950 (2011).
- [40] L. E. Fischer, M. Leahy, A. Eddins, N. Keenan, D. Ferracin, M. A. Rossi, Y. Kim, A. He, F. Pietracaprina, B. Sokolov, *et al.*, arXiv preprint arXiv:2411.00765 (2024).
- [41] M. Rennela and H. Ollivier, arXiv preprint arXiv:2411.06422 (2024).

Appendix A: pPEC via MCMC method

Here we give a description on how to estimate a global inverse noise channel via a Markov Chain Monte Carlo (MCMC) simulation. While in general this approach is not scalable and applicable only to small system sizes it serves as an excellent educational example on how the interference of corrections reduces the sampling overhead.

The key insight to understand how the combination of channels reduces the sampling overhead lies in the interference of corrections. Considering for example a layer where a specific correction P_i has been sampled, it is possible that the effect of the correction is exactly canceled by a subsequent correction P_j , so that the same global correction could be achieved by performing no correction at all.

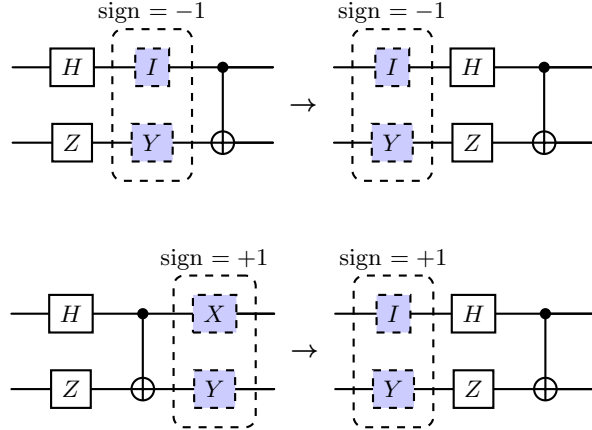


FIG. 7: Example of interfering error paths. The drawn corrections (dashed blue gates) of the individual error paths amount, after the propagation, to the same correction although at a different sign. Calculating both paths is thus superfluous, since their contribution to the average can be easily accounted for in preprocessing.

A simple graphical illustration of interfering corrections is shown in fig. 7. In this simplified model two corrections are drawn which lead to the same global correction, although at a different global sign. In the average this pair of paths cancels each other in the average and can be omitted from sampling.

To quantify the amount of interference we utilize a MCMC algorithm that iterates reversely over each noisy layer in the circuit, drawing a specific Pauli correction P_l and corresponding sign s_l at each step. Consecutively, the drawn correction is propagated behind the next gate layer using a look-up table (appendix. B) $P_l \rightarrow \tilde{P}_l$. At the next gate layer, a new Pauli correction P_{l-1} and sign s_{l-1} are drawn, which get multiplied with the propagated Pauli correction $P_{\text{prod}} = \tilde{P}_l P_{l-1}$ and the previous sign $s_{\text{prod}} = s_l s_{l-1}$. Then the product of the Pauli operators P_{prod} is propagated to the next layer, where the same process is repeated until the last noisy layer (or the initialization of the qubits) is reached.

As described in sec. III A, at the initialization or the measurement layer, the corrections Y can be replaced by X and Z by I in each sampled final Pauli correction string via the XI-reduction.

Finally, each time a specific correction P_{final} was sampled, we save the number of occurrences and increment or decrement the index of draws depending on s_{final} . In this way, some corrections may interfere constructively, while others interfere destructively. Using this procedure the reduction in the sampling overhead can be estimated by considering the amount of path interference

$$\frac{\gamma_{\text{ppec}}}{\gamma} = \frac{\# \text{ paths total} - \# \text{ interfering paths}}{\# \text{ paths total}}, \quad (\text{A1})$$

where a *path* refers to one iteration of the MCMC algorithm, in which the corrections have been propagated to the start or end of the circuit and a final global correction has been registered.

It is important to note that, due to the sign problem of the MCMC approach with quasi probability distributions, the number of Monte-Carlo samples needs to be scaled accordingly to address deep circuits.

Algorithm 1 Monte-Carlo Simulation to estimate the global inverse

```

while  $n < \text{samplesize}$  do
  while layer index  $\neq 0$  do
    layer corr, sign  $\leftarrow$  sample correction and sign
    if layer index = N then
      global corr  $\leftarrow$  layer corr
      global sign  $\leftarrow$  sign
      Continue
    end if
    global corr  $\leftarrow$  propagate correction
    global corr  $\leftarrow$  global corr  $\times$  layer corr
    global corr sign  $\leftarrow$  global sign  $\times$  sign
    layer index  $\leftarrow$  layer index - 1
  end while
  Replace Y with X and Z with I in global correction
  add global sign  $\times$  global correction to dictionary
end while

```

After the estimation of the global inverse, PEC can be performed by drawing from the estimated distribution obtained from the MCMC simulation. For a fixed number of circuit instances a correction and corresponding sign are drawn, and the results are multiplied with the corresponding sign and averaged. Finally, the results need to be rescaled by the corresponding γ -factor. Due to the path interference, the total γ factor now amounts to

$$\gamma_{\text{pec}} = \gamma \cdot \frac{\# \text{ samples} - \# \text{ interfering samples}}{\# \text{ samples}}, \quad (\text{A2})$$

showing the same structure as eq. 14.

Note that due to the exponential scaling of the correction space, this approach requires an exponentially scaling amount of Monte-Carlo samples in order to converge. To circumvent prohibitive classical costs, the method can be truncated by for example only considering a select number of layers or performing the channel products analytically for a select set of channels.

Appendix B: Commutation Tables for Clifford Gates

In this section we showcase the basic commutation tables for the most used gates of the Clifford group of dimension $n = 1$ and $n = 2$. While it is generally true that each element of the Clifford group can be decomposed into H , S and C_X gates we provide commutation tables for a larger set of gates, since they are customary used in some decompositions or native gate sets of quantum hardware (such as the basis $\{X, S_x, R_z, C_X\}$).

II	II
IX	XX
IY	XY
IZ	IZ
XI	XI
XX	IX
XY	IY
XZ	XZ
YI	YZ
YX	ZY
YY	ZX
YZ	YI
ZI	ZZ
ZX	YX
ZY	XY
ZZ	ZI

II	II
IX	ZX
IY	ZY
IZ	IZ
XI	XZ
XX	YY
XY	YX
XZ	XI
YI	YZ
YX	XY
YY	XX
YZ	YI
ZI	ZI
ZX	IX
ZY	IY
ZZ	ZZ

II	II
IX	XI
IY	YI
IZ	ZI
XI	IX
XX	XX
XY	YX
XZ	ZX
YI	IY
YX	XY
YY	YY
YZ	ZY
ZI	IZ
ZX	XZ
ZY	YZ
ZZ	ZZ

H-Commutaion table	
I	I
X	Z
Y	Y
Z	X

S_X -Commutaion table	
I	I
X	X
Y	Z
Z	Y

S_Y -Commutaion table	
I	I
X	Z
Y	Y
Z	X

S_Z -Commutaion table	
I	I
X	Y
Y	X
Z	Z

TABLE I: Commutation tables for the most used gates of the Clifford group. The commutation tables were calculated via the relation $P' = CPC^\dagger$.

Appendix C: Conjoint implementation of inverse noise channels

We provide a simple prove that it is always favorable in terms of the sampling overhead to multiply two inverse Pauli channels together before probabilistically implementing them. We start the proof by considering a general inverse Pauli noise channel

$$\Lambda^{-1}(\rho) = \sum_{i=1}^{4^n} a_i P_i \rho P_i^\dagger = \sum_{i=1}^{4^n} a_i \mathcal{P}_i \quad a_i \in \mathbb{R} \quad (\text{C1})$$

where $\mathcal{P}_i(\rho) \triangleq P_i \rho P_i^\dagger$ denotes the Kraus channel representation of a Pauli P_i . Considering that the sampling overhead γ is calculated by

$$\gamma(\Lambda^{-1}) = \gamma\left(\sum_{i=1}^{4^n} a_i \mathcal{P}_i\right) = \sum_{i=1}^{4^n} |a_i| \quad (\text{C2})$$

it is easy to verify that the sampling overhead of implementing two inverse noise channels is given by

$$\gamma(\Lambda_1^{-1})\gamma(\Lambda_2^{-1}) = \sum_{i,j=1}^{4^n} |a_i||b_j|. \quad (\text{C3})$$

On the other hand multiplying both inverses, before calculating the sampling overhead, yields

$$\begin{aligned} \gamma(\Lambda_1^{-1}\Lambda_2^{-1}) &= \gamma\left(\sum_{i=1}^{4^n} a_i \mathcal{P}_i \sum_{j=1}^{4^n} b_j \mathcal{P}_j\right) \\ &= \gamma\left(\sum_{k=1}^{4^n} \left(\sum_{i,j}^{4^n} a_i b_j \xi_{ijk}\right) \mathcal{P}_k\right) \quad \text{with} \quad \xi_{ijk} = \begin{cases} 1 & \text{if } \mathcal{P}_i \mathcal{P}_j = \mathcal{P}_k \\ 0 & \text{otherwise} \end{cases} \\ &= \sum_k^{4^n} \left(|\sum_{i,j}^{4^n} a_i b_j \xi_{ijk}|\right) \\ &\leq \sum_k^{4^n} \left(\sum_{i,j}^{4^n} |a_i||b_j||\xi_{ijk}|\right) \\ &= \sum_{i,j=1}^{4^n} |a_i||b_j| = \gamma(\Lambda_1^{-1})\gamma(\Lambda_2^{-1}), \end{aligned} \quad (\text{C4})$$

where we made use of the triangle inequality as well as the fact that the total number of terms $a_i b_j$ needs to be conserved by the summation over k , i.e. ξ_{ijk} contains only one non-zero element for each product $\mathcal{P}_i \mathcal{P}_j$, $\sum_k |\xi_{ijk}| = 1$

$\forall i, j$. Thus, the cost of implementing two inverse channels separately is always greater or equal than the conjoint implementation. Note that in contrast to taking the product of two Pauli observables, the phase of the product of two Pauli channels can be omitted since $(e^{i\phi}P)\rho(e^{i\phi}P)^\dagger = P\rho P^\dagger$.

Appendix D: Symmetrization of readout errors

We consider a readout error which is described by a tensor product noise model

$$A = \bigotimes_{i=1}^n A^i = \bigotimes_{i=1}^n \begin{bmatrix} 1 - \epsilon_i & \eta_i \\ \epsilon_i & 1 - \eta_i \end{bmatrix}, \quad (\text{D1})$$

meaning that the errors on each qubit occur independently. The measurement is described by a set of projectors $\pi_m = |m\rangle\langle m|$, which project onto the computational basis. The noisy projection operators are then given by

$$\tilde{\pi}_m = \sum_n A_{mn} |n\rangle\langle n| \quad (\text{D2})$$

where $A_{mn} = \langle m|A|n\rangle$ are the matrix elements of the error matrix. For the considered noise model the matrix A is sparse with only few non-vanishing matrix elements. The randomized insertion of X gates (and correction in post-processing) leads to a twirled readout error [27] given by

$$A_{\text{twirl}} = \frac{1}{2^n} \sum_{s \in \{0,1\}^n} X^{\otimes s} A X^{\otimes s, \dagger} \quad (\text{D3})$$

where the $X^{\otimes s}$ operator corresponds to bit flips of the qubits indexed by s . Since the considered noise model does not contain contributions of cross talk it suffices to consider each single qubit error A^i twirled under a single X separately

$$\begin{aligned} A_{\text{twirl}}^i &= \frac{1}{2} (A^i + X A^i X^\dagger) \\ &= \frac{1}{2} \left(\begin{bmatrix} 1 - \epsilon_i & \eta_i \\ \epsilon_i & 1 - \eta_i \end{bmatrix} + \begin{bmatrix} 0 & 1 \\ 1 & 0 \end{bmatrix} \begin{bmatrix} 1 - \epsilon_i & \eta_i \\ \epsilon_i & 1 - \eta_i \end{bmatrix} \begin{bmatrix} 0 & 1 \\ 1 & 0 \end{bmatrix} \right) \\ &= \frac{1}{2} \left(\begin{bmatrix} 1 - \epsilon_i & \eta_i \\ \epsilon_i & 1 - \eta_i \end{bmatrix} + \begin{bmatrix} 1 - \eta_i & \epsilon_i \\ \eta_i & 1 - \epsilon_i \end{bmatrix} \right) \\ &= \begin{bmatrix} 1 - p_x & p_x \\ p_x & 1 - p_x \end{bmatrix} \\ &= (1 - p_x) \begin{bmatrix} 1 & 0 \\ 0 & 1 \end{bmatrix} + p_x \begin{bmatrix} 0 & 1 \\ 1 & 0 \end{bmatrix} \end{aligned} \quad (\text{D4})$$

with $p_x = \frac{\epsilon_i + \eta_i}{2}$. Hence the randomized insertion of X gates transforms a general single qubit readout error channel into a Pauli X error channel.

We would like to note, that the method straight forwardly generalizes to either the full readout error matrix or a model considering crosstalk of a subset of qubits. The integration of larger matrices comes at the cost of estimating each correlated measurement, but might generally reduce or even fully eliminate any bias.

Appendix E: pPEC for SPL noise models

We now consider pPEC applied to Sparse-Pauli-Lindbladian (SPL) noise models. These models can be efficiently stored in a product representation of individual model Paulis which only model interactions between physically connected qubits. We depart from the product representation of an inverse Pauli channel as given in ref [19]

$$\Lambda^{-1}(\rho) = \prod_{k \in \mathcal{K}} (w_k \mathcal{I}(\cdot) - (1 - w_k) \mathcal{P}_k(\cdot)) \rho. \quad (\text{E1})$$

Akin to the dense representation, the quasi probability implementation of the inverse channel is attached to a cost factor γ . For the SPL model the γ -factor is given by

$$\gamma = \prod_{k \in \mathcal{K}} (2w_k - 1)^{-1}, \quad (\text{E2})$$

which we aim to reduce using pPEC. Applying the pPEC method, each of the individually commuting Pauli channels is propagated to the start of the circuit by taking its conjugation with the circuit operation up to the select inverse channel

$$\begin{aligned} \tilde{\Lambda}^{-1}(\rho) &= \prod_{k \in \mathcal{K}} (w_k \mathcal{C}(\mathcal{I})(\cdot) - (1 - w_k) \mathcal{C}(\mathcal{P}_k)(\cdot)) \rho \\ &= \prod_{k \in \mathcal{K}} (w_k \mathcal{I}(\cdot) - (1 - w_k) \tilde{\mathcal{P}}_k(\cdot)) \rho \end{aligned} \quad (\text{E3})$$

where \mathcal{C} denotes the Clifford circuit operation up to the respective inverse error channel and the operator $\tilde{\mathcal{P}}_k = \mathcal{C} \mathcal{P}_k \mathcal{C}^\dagger \cdot \mathcal{C}^\dagger \mathcal{P}_k^\dagger \mathcal{C}$ denotes the conjugated Pauli channel. Applying this procedure to each correction layer, the global inverse is given by

$$\Lambda_{\text{global}}^{-1} = \prod_l \tilde{\Lambda}_l^{-1} = \prod_{k \in L \cdot \mathcal{K}} (w_k \mathcal{I}(\cdot) - (1 - w_k) \tilde{\mathcal{P}}_k(\cdot)) \rho \quad (\text{E4})$$

where the index k now runs over all model Paulis for the total number of layers L , yielding a total of $L \cdot |\mathcal{K}|$ terms.

Again as in the MCMC approach a further reduction can be achieved by utilizing the XI-reduction. In this model it suffices to replace the operators Y by X and Z by I in each of the individual Pauli channels in the product. As an immediate improvement all channels, which contain only Z and I Pauli operators can be directly omitted from the inverse noise channel and do not contribute to the sampling overhead, since

$$(w_k \mathcal{I} - (1 - w_k) \mathcal{I}) = (2w_k - 1) \mathcal{I} \quad (\text{E5})$$

directly cancels with the corresponding term $(2w_k - 1)^{-1}$ in the γ factor. We denote this as *passive reduction*.

The global inverse noise channel will in general contain multiple Paulis that have been mapped to the same operator. The amount of terms in the product can then be directly reduced by multiplying terms with equal Paulis together

$$\begin{aligned} (w_1 \mathcal{I} - (1 - w_1) \mathcal{P}) \cdot (w_2 \mathcal{I} - (1 - w_2) \mathcal{P}) &= (w_1 w_2 + (1 - w_1)(1 - w_2)) \mathcal{I} - (w_1(1 - w_2) + (w_2(1 - w_1))) \mathcal{P} \\ &= w_3 \mathcal{I} - (1 - w_3) \mathcal{P}. \end{aligned} \quad (\text{E6})$$

Since generally

$$(2w_1 - 1)^{-1} (2w_2 - 1)^{-1} = (2w_3 - 1)^{-1} \quad (\text{E7})$$

this multiplication does not reduce the sampling overhead γ but can drastically reduce the number of total terms in the product.

As explained in ref. [19] a further decrease in the sampling overhead can be achieved by explicitly expanding the product of eq. E4

$$\Lambda^{-1}(\rho) = \prod_{k \in \mathcal{K}} (w_k \mathcal{I}(\cdot) - (1 - w_k) \mathcal{P}_k(\cdot)) \rho \rightarrow \sum_i c_i \mathcal{P}_i(\rho). \quad (\text{E8})$$

Due to the multiplication of equal Pauli channels as well as the larger number of terms in this product, this expansion will yield far more drastic reductions than the expansion of an individual inverse channel given by eq. E1.

In the worst case the expansion will result in an exponential growth in the number of required parameters to characterize the noise channel. This leads to a general tradeoff between required classical and quantum resources. However, the growth in the number of required coefficients can be reduced by utilizing specific term orderings before the expansion.

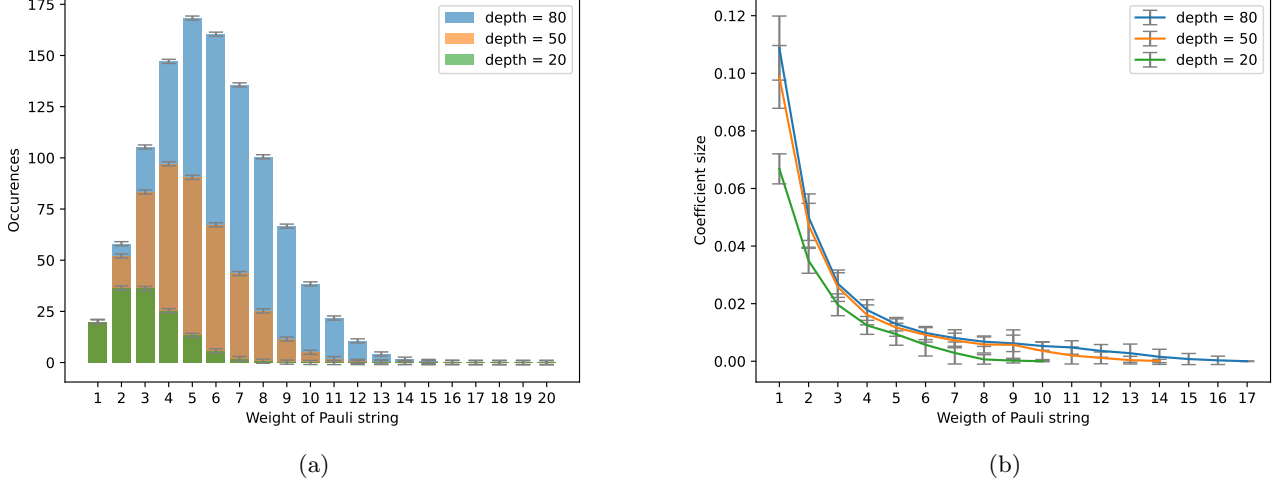


FIG. 8: Absolute value of coefficients and weights of the model Paulis for different circuit depths. The data is averaged over several instances of random Clifford circuits of 20 qubits. (a) Amount of Pauli strings relative to the number of non identity terms. For deeper circuits more Paulis with a higher weight are present. (b) Absolute value of the coefficient $|(1 - w_k)|$ of the different Pauli strings after propagation relative to the amount of non identity terms in the Pauli string.

Appendix F: Efficient expansion of SPL noise models

As stated in ref. [19] the product structure of the noise model in SPL form can be explicitly expanded to reduce the sampling overhead γ , although at a computational cost in compute time as well as memory.

The number of required parameters and multiplications for the model scales quasi exponentially, meaning that each into the sum absorbed term can in theory double the number of required coefficients. To evade this exponential increase the expansion can be truncated cutting the multiplication off at a selected index

$$\Lambda^{-1}(\rho) = \prod_{k' \in \mathcal{K}'} (w_{k'} \mathcal{I}(\cdot) - (1 - w_{k'}) \mathcal{P}_{k'}(\cdot)) \left(\sum_i c_i \mathcal{P}_i(\cdot) \right) \rho. \quad (\text{F1})$$

The reduction in the sampling overhead can then be estimated by calculating the γ -factor of the expanded inverse channel

$$\gamma_{\text{reduction}} = \sum_i |c_i| \leq 1, \quad (\text{F2})$$

which is less or equal to 1 due to interference. While this approach is generally computationally more bearable, a direct expansion of the product, without exploiting structure, is still taxing and often inefficient. This inefficiency can be explained by considering a single expansion step

$$(w_i \mathcal{I} - (1 - w_i) \mathcal{P}_i) \left(\sum_k c_k \mathcal{P}_k \right) = \left(w_i \sum_k c_k \mathcal{P}_k \mathcal{I} - (1 - w_i) \sum_k c_k \mathcal{P}_k \mathcal{P}_i \right), \quad (\text{F3})$$

which leads to two separate sums, doubling the number of required coefficients. The amount of coefficients will however only double if no terms in the two sums are equal, that is no terms interfere. Luckily this case is not of interest for pPEC, since the reduction in sampling overhead exactly stems from this interference.

One approach to maximize the amount of interference is the utilization of the subgroup structure of the Pauli operators. As a basic example, consider the expansion of the three single qubit Pauli channels

$$(w_1 \mathcal{I} - (1 - w_1) \mathcal{X})(w_2 \mathcal{I} - (1 - w_2) \mathcal{Y})(w_3 \mathcal{I} - (1 - w_3) \mathcal{Z}) = (1 - p_1 - p_2 - p_3) \mathcal{I} + p_1 \mathcal{X} + p_2 \mathcal{Y} + p_3 \mathcal{Z} \quad (\text{F4})$$

which can be expanded without any increase in the number of coefficients. The cursive operators indicate that the operators act as channels in Kraus representation i.e. $\mathcal{X} = X(\cdot)X^\dagger$. The same holds trivially for any larger subgroup,

as for example the 15 parameter group of $n = 2$, the 63 parameter group of $n = 3$ as well as any higher dimensional subgroup.

Further, the propagation of Paulis through deep circuits will lead to high weight Paulis as demonstrated in fig. 8 (a). On the other hand, the size of the coefficients w_k is far smaller than those of low weight operators (fig. 8 (b)) since it is highly unlikely that two corrections are mapped to the same high weight operator. Since the general reduction of the expansion is dependent on the magnitude of the channel coefficients, the absorption of low weight Paulis is more favorable.

Based on these heuristics we define a more efficient expansion of the product as follows. We start by ordering the terms in lexicographical ordering [25]

$$\begin{aligned} III &\preceq IIX \preceq IYY \preceq IIZ \\ &\preceq IXI \preceq IXX \preceq IXY \preceq IXZ \\ &\preceq IYI \preceq IYX \preceq IYY \preceq IYZ \preceq \dots \end{aligned} \quad (\text{F5})$$

and expanding the product of the first two terms. In each consecutive step we absorb a term only if its support is also in the continuously growing expanded inverse noise channel. If no Pauli with the same support is found, the next Pauli in the ordering is chosen.

Generally, after expanding the first truncated sum, the process can be iteratively applied to the remainder of the product, yielding several partially expanded sums

$$\Lambda^{-1}(\rho) = \prod_{k \in \mathcal{K}} (w_k \mathcal{I}(\cdot) - (1 - w_k) \mathcal{P}_k(\cdot)) \rho \rightarrow \left(\sum_{i_1} c_{i_1} \mathcal{P}_{i_1}(\cdot) \right) \left(\sum_{i_2} c_{i_2} \mathcal{P}_{i_2}(\cdot) \right) \dots \left(\sum_{i_N} c_{i_N} \mathcal{P}_{i_N}(\cdot) \right) \rho. \quad (\text{F6})$$

Using this process the inverse channel can be expanded into multiple smaller sums, each with only a limited number of terms and total sampling overhead

$$\gamma_{\text{pPEC}} = \gamma \prod_{j=1}^N \sum_i |c_{i_j}|. \quad (\text{F7})$$

While we do find that the lexicographical ordering leads to significant reductions it is possible that other orderings might lead to even more interference.